A Solidly Mounted 55 GHz Overmoded Bulk Acoustic Resonator

Zachary Schaffer, Ahmed Hassanien, Mohammad Ayaz Masud, Gianluca Piazza
Department of Electrical and Computer Engineering
Carnegie Mellon University
Pittsburgh, PA
zschaffer@cmu.edu

Abstract—In this work we present a solidly mounted overmoded bulk acoustic resonator (OBAR) designed to operate at millimeter wave (mmWave) frequencies. This device uses a combination of overmoded operation, a layer transfer based fabrication process, all metal Bragg mirrors, and series arrays to allow acoustic resonator frequency scaling through V band. The solidly mounted OBAR can have up to 2/3 the kr^2 of a fundamental mode (~4% for AlN, >10% for ScAlN or LN), reasonable piezoelectric film thicknesses (>100 nm at 50 GHz for AlN), arbitrarily thick electrodes to minimize ohmic loss, and be made in series arrays to allow 50 Ω matched devices with reasonable area to perimeter ratios. We demonstrate a proof of concept device using a 110 nm AlN piezoelectric layer operating at 55 GHz with an electromechanical-coupling coefficient (kr^2) of 2.2%, and a series resonance quality factor (Qs) of 90.

Keywords—Acoustic resonator, mmWave resonator, piezoelectric resonators, solidly mounted resonator, overmoded bulk acoustic resonator

I. INTRODUCTION

There is rapidly growing interest in acoustic resonators as an approach to filtering signals in the millimeter-wave (mmWave) frequency spectrum. Existing mmWave filtering relies on electromagnetic (EM) resonators that are unable to provide the footprint required for applications such as per element filtering of phased array antennas. Acoustic resonators have become the de facto standard in the sub 8 GHz frequency range [1], show promising results in the 8-18 GHz range, and provide a possible pathway to practical mmWave filters [2].

Acoustic resonators need high electromechanical-coupling coefficient (k_t^2) to synthesize filters with low insertion loss and wide enough passbands, high quality factor (Q) to minimize insertion loss, maximize roll-off, and have reasonable footprints at the 50 Ω characteristic impedance required to match prior and subsequent radio frequency (RF) front end elements. Scaling acoustic resonators to mmWave, while maintaining these properties brings significant challenges. Primarily, scaling up frequency requires scaling down film thickness and device area. Attempting to use the fundamental thickness mode bulk acoustic wave resonators (BAWs) that dominate sub 6 GHz at 50 GHz, requires impractically thin piezoelectric films, area to perimeter ratios that make lateral leakage unmanageable, and thin electrodes that result in extreme ohmic loss (low Os) [2]. Scaling efforts using a fundamental thickness mode have been demonstrated up to 20 GHz using high quality sputtered films [3] and the use of a fully epitaxially grown stack may allow close to single crystal bulk properties in ultra-thin films pushing scaling to its limit [4]. However, lateral leakage and ohmic loss ultimately limit the frequency achievable with a fundamental thickness mode.

One alternative is to operate devices in an overtone instead of a fundamental mode, which allows increased piezoelectric thickness at the cost of reduced k_t^2 due to internal charge cancellation. With high coupling materials such as lithium niobate (LN), this can still produce reasonable k_t^2 devices [5]. k_t^2 reduction due to charge cancellation may be avoidable through the use of periodically poled piezoelectric films (P3F), but this introduces significant fabrication challenges. P3F devices have been demonstrated in LN using multiple thin film transfers to demonstrate a notable 7.3% k_t^2 at 57 GHz [6], and in AlN/ScAlN using either ScAlN ferroelectric properties to pole films by an externally applied voltage [7] or the use of different deposition techniques (PVD vs MoCVD) that grow opposite orientation films [8]. While P3F approaches help with film thickness and area to perimeter ratio scaling problems, ohmic loss is still an issue for thickness modes. Lateral field excitation methods to excite two dimensional mode overtones in ScAlN [9] or antisymmetric plate mode overtones in LN [10] can help better manage ohmic loss, but the use of interdigital transducer based electrodes presents significant challenges for setting device frequency in a production environment and device characteristic impedance is often far higher than 50 Ω , which would require external matching passives. We have previously demonstrated a released 33 GHz Overmoded Bulk Acoustic Resonator (OBAR) that relies on a single orientation piezoelectric layer operating in an overmode where energy is shared equally between the piezoelectric and similar thickness metal layers, providing reasonable thickness electrodes in a thickness mode.

We refine this approach with additional design elements to demonstrate a solidly mounted OBAR. Unlike released OBARs, these devices are fully encapsulated with all metal Bragg mirrors, allowing for a solidly mounted design with arbitrarily thick electrodes. In this work, we demonstrate an AlN based proof of concept device operating at 55 GHz with 2.2% k_t^2 and 90 Qs. Correction of film thickness fabrication errors could improve k_t^2 above 3% and the use of a high coupling piezoelectric material such as ScAlN or lithium niobate (LN) could improve k_t^2 beyond 10%.

II. DESIGN AND SIMULATION

A. Principle of Operation

Multiple novel design elements come together in the solidly mounted OBAR. First, optimization of the acoustically active electrode through the use of an inner low acoustic impedance (Z) and outer high Z layer allow overmode operation with 2/3 the k_t^2 of the fundamental mode instead of the 1/3 k_t^2 achievable using a uniform Z stack. The selection of low loss metals for the main cavity helps to maintain device Q. Second, the use of a layer transfer based fabrication process allows for high quality piezoelectric thin films not grown on the bottom electrode, and models show ~4% k_t^2 is achievable using pure AlN and >10% k_t^2 is achievable using high coupling materials such as LN or ScAlN films. Third, the use of dual, all metal Bragg mirrors decouples the thickness scaling needed to upscale frequency from electrode thickness, making ohmic loss manageable. This also results in a solidly mounted device with arbitrarily thick metal routing on both sides. This should provide excellent mechanical robustness and power handling though these were not modeled or tested in this work. Fourth, with very low electrical resistance, it becomes practical to create cascaded series arrays of resonators, allowing individual resonators to have reasonable area to perimeter ratios while still producing a 50 Ω characteristic impedance device. This is especially important for high permittivity materials such as ScAlN and LN that—without cascading—would need <30 µm² device areas at 50 GHz.

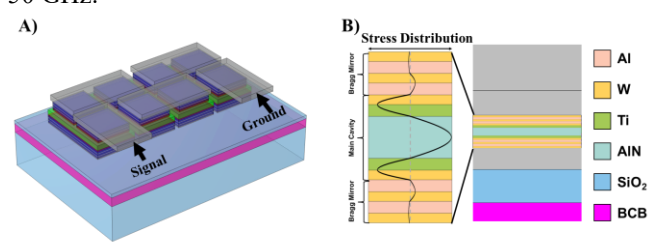


Fig. 1. A) Isometric schematic of solidly mounted overmoded bulk acoustic resonator (OBAR) array consisting of 8 series cascaded elements. B) Cross section of acoustic cavity with overlay of stress distribution.

Operating a resonator at an overtone above the fundamental mode allows a higher frequency for the same thickness, at the cost of k_t^2 reduction due to a combination of internal cancellation of generated charge and increased acoustic load. The overmode approach extends overtones into the top and bottom metal electrodes, operating in a 3rd harmonic, making a total 3/2 wavelength (λ) cavity. Neglecting Z mismatch effects, metal electrode thickness is now $1/2 \lambda$ (same as the piezoelectric layer) instead of as thin as possible. This results in a mode with 1/3 the k_t^2 of the fundamental mode instead of the $1/9 k_t^2$ achievable with a standard 3rd harmonic. Optimization of the electrode can double k_t^2 compared to the uniform Z, uniform thickness case. This is possible by increasing the ratio of electrode to piezoelectric thickness (rep) to be slightly more than 1/3 to increase charge density in the central piezoelectric layer, as well as using electrodes with a low Z inner layer and high Z outer layer. The low Z inner layer reduces acoustic loading while the high Z outer layer serves to better confine acoustic energy to the AlN layer as the mode shape is flattened out.

We select a Ti/W pair for the electrode based on acoustic impedance mismatch, and an expectation of higher mechanical *Q* for Ti than Al. If not using all metal Bragg mirrors, electrical conductivity should also be considered.

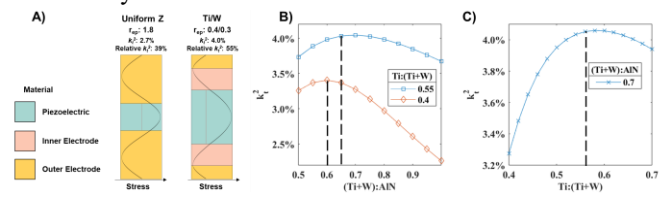


Fig 2. A) Cross section with stress distribution for uniform acoustic impedance and Ti/W overmodes with optimal electrode to piezoelectric thickness ratios (r_{ep}) . B/C) k_i^2 dependence on layer thickness ratios determined by FEA.

Bragg mirrors function using a series of interfaces with mismatched acoustic impedance (Z) precisely spaced so that reflections constructively interfere. These are often implemented using a high Z metal and low Z dielectric [1]. If instead both high and low Z materials are metal, the acoustic cavity of the device can be thin while keeping a thick metal layer to minimize ohmic loss. By solidly mounting a resonator, robustness to shock is improved compared to a released device and heat can be conducted directly down to the substrate instead of laterally through a suspended thin film, improving power handling. A second Bragg mirror can be used on the topside of the resonator to fully encapsulate the device [11], and thicken the top metal in our case. Bragg mirror performance is dependent on the mismatch of Z between layers. With the Ti/W pair main cavity electrode functioning similar to a Bragg mirror, little mechanical energy enters the first layer of our Bragg mirror making the use of low mechanical Q metals such as Al reasonable. We use an Al/W pair for our Bragg mirrors considering electrical conductivity, acoustic impedance mismatch, and our deposition capabilities. FEA simulations of transmission through the Bragg mirror were used to optimize layer thickness, with an optimal result of 32 nm of Al and 26 nm of W, which corresponds to roughly $1/4 \lambda$ sizing. Mirror transmission is shown to be wide band enough that a small frequency error should not shift results, but narrow enough that the fundamental mode at 18 GHz will be leaked to substrate, and therefore suppressed. This results in a single transduced mode, an improvement over previously demonstrated released OBARs which have a well transduced fundamental mode [38].

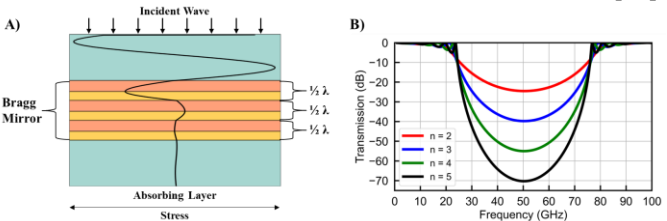


Fig. 3. A) Finite element analysis model setup for simulation of Bragg mirror transmission with overlay of stress distribution. B) Results of simulation for Al/W pair showing mirror transmission vs number of Bragg mirror pairs (n).

B. Device Modeling

We use FEA to model k_t^2 and mechanical energy distribution throughout the stack. Mechanical energy distribution is then combined with per material models of

quality factor to determine an intrinsic mechanical quality factor for the device using:

$$Q_{intrnisic} = \frac{U_{tot}}{\frac{U_1}{Q_1} \dots + \frac{U_n}{Q_n}}$$

where U is mechanical energy and subscripts 1 through nrepresent each material in the stack. Per material quality factors are calculated considering thermoelastic damping, phonon phonon interactions, and phonon electron interactions using analytical models detailed in [12]. Measurements of mechanical loss Al thin films up to 25 GHz have shown good alignment to this approach [13], but generally characterization of metal thin film mechanical loss for mmWave is lacking. Measured Q in 33 GHz released OBARs and the 55 GHz OBARs in this work was significantly worse than models predicted, possibly due to unmodeled defect and boundary scattering losses. Fig. 4. shows a comparison of per material Q, and simulation of device Q showing frequency scaling and the impact of layer errors from the fabricated stack. Based on these results, mechanical Q of the main cavity metals (Ti and W) is expected to set device Q, and ~ 5 nm errors in Ti and W thickness reduce k_t^2 significantly.

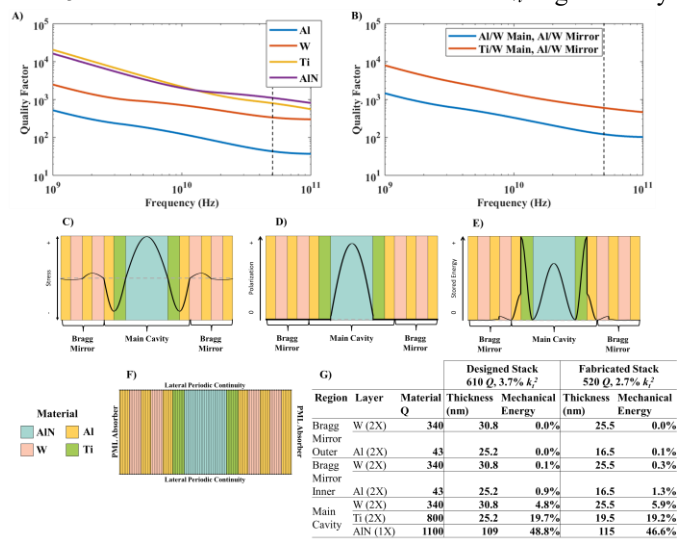


Fig. 4. Cross section of acoustic resonator main cavity with overlay of A) stress, B) piezoelectric polarization, C) mechanical energy, and D) model setup. E) Per layer material, quality factor, mechanical energy distribution, and resulting k_t^2 and Q are also shown.

III. DEMONSTRATION

A. Fabrication

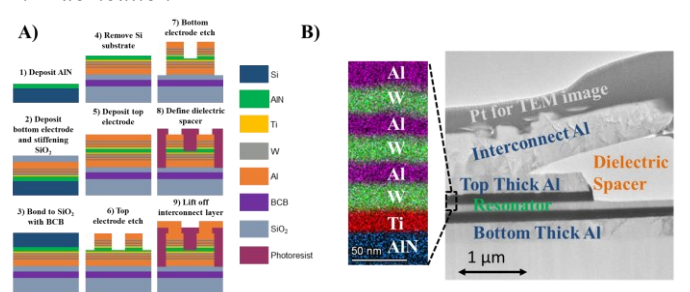


Fig 5. A) Cross section of film transfer based fabrication process. B) Cross sectional TEM of fabricated device with high magnification insert colored by EDX.

Devices are fabricated using a 9 step, 3 mask process shown in 5. (1) The 110 nm AlN layer is deposited on an Si handler wafer using a reactive cosputter tool with a low power recipe optimized for ultra-thin films. (2) The bottom active metals, all metal Bragg mirror and thick Al routing layer (400nm) are then sputter deposited followed by a SiO₂ (1.6 μm) stiffening layer. (3) In the next step, the initial Si die with deposited layers is flip chip bonded to a new fused silica die using a BCB interface layer. After the bonding process BCB was very stable, and found to be resistant to > 12 hour exposure to wet solvents such as acetone, IPA, and 1165 heated to 80 °C. (4) The Si handler is then thinned from 500 to 50 µm using SF₆/O₂ RIE, cleaned of etch residues, and then the final Si is removed using XeF₂ to prevent surface damage to the AlN film. (5) The top active metals, all metal Bragg mirror and thick Al routing layer (400 nm) is then sputter deposited. (6) Ion milling is then used to define the top electrode. We stop in the middle of the AlN layer to prevent any shorting between top and bottom electrode due to redeposition. (6) A second ion milling step is used to define the bottom electrode, stopping on the SiO₂ stiffening layer. (7) Photoresist is then used as a planarization and spacer layer by spinning, pattering, and then hard baking to fully cross link. (8) Finally, a thick (1.5 µm) Al interconnect layer is deposited and patterned using liftoff. This Al layer fills the holes left in the photoresist, connects devices together for series arrays, and is contacted by probes to allow measurements. Real film thickness was determined after fabrication by cross sectional TEM, and ~5 nm errors resulted due to challenges in deposition rate characterization.

B. Results

We present a device comprised of 2 series cascaded 11µmx11µm square resonators. An Agilent PNA-X is used in a thru configuration with two 100 µm pitch GSG probes. An off chip Short Open Load Thru (SOLT) calibration was used to extend reference plane to the probe tips, and an on chip short formed by only the thick interconnect routing layer is used to remove contact resistance and parasitic inductance. Broadband response was determined based on calibration and measurement from 1 to 65 GHz, while main mode response was determined based on calibration and measurement from 45 to 65 GHz. Device response is fit to a mBVD model, as there are no significant spurious modes, and Bode *Q* calculated [14].

Broadband response is shown in Fig. 6. The response is free of other modes, allowing filter implementations without external suppression. As predicted, the Bragg mirrors are transmissive at the fundamental mode frequency (~18 GHz) leaking it to the substrate. The second and fourth harmonic are not transduced since they are even and charge within the piezoelectric layer cancels. The fifth harmonic is expected to occur at ~92 GHz which is beyond our measurement range, but should also be suppressed by the Bragg mirrors.

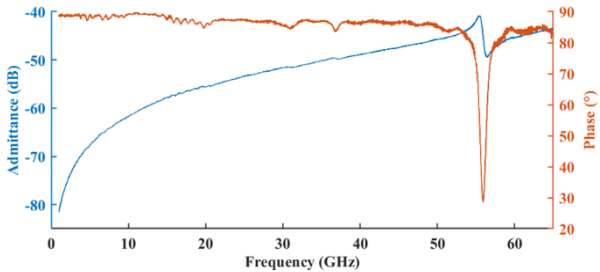


Fig. 6. Resonator wideband response showing lack of spurious modes up to 65 GHz

Main mode characteristic response is shown in Fig. 7, with overlay of mBVD model fit and Bode Q. Bode Q indicates presence of a spurious mode before f_s not clearly visible from admittance, but shows clear response in band.

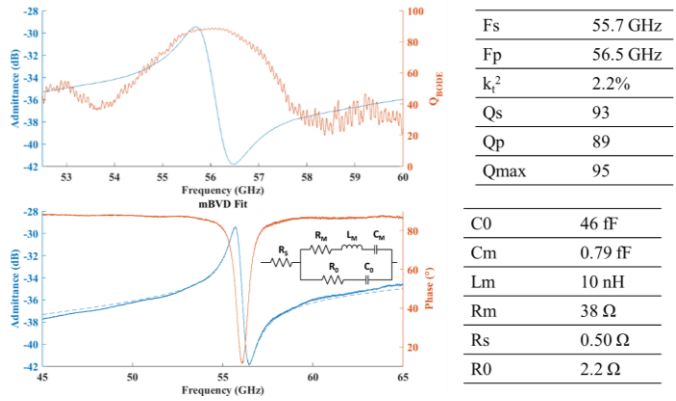


Fig 7. Measured resonator electrical response showing admittance, Bode Q, mBVD fitting, and derived metrics.

Measured k_t^2 of 2.2% was 20% lower than the simulated 2.7% value for the fabricated stack thickness. This is likely due to quality degradation in the ultra-thin 110 nm AlN film. Os. Op, and max Bode Q are very close, indicating contributions from additional loss terms at f_s and f_p (R_s and R₀) are not dominant. The modeled electrode resistance of 0.6Ω for this geometry fit closely to the mBVD fit value of 0.5 Ω and works out to <2% of the 38 Ω R_m, making ohmic loss minimal. At parallel resonance we consider dielectric loss reported as tanδ. We estimate $tan\delta$ by taking the real component of out of band impedance then removing the $0.6 \Omega R_s$ value modeled by HFSS. From this we extract a $\tan \delta$ which increases linearly from 3-6% between 45 and 65 GHz, a similar frequency dependence to 1-10 GHz measurements of ScAlN tanδ [15]. This works out to ~7% loading for Qp. From this we conclude device Q is limited by phononic loss, presumably in the main cavity Ti/W electrodes.

IV. CONCLUSION

In this work we introduced a solidly mounted overmoded bulk acoustic resonator (OBAR) as a practical approach to scaling acoustic resonators to mmWave frequencies. We demonstrate a proof of concept device that is ~50 Ω matched and operates at 55 GHz with, 2.2% k_t^2 and ~90 Qs and Qp. For the same design, k_t^2 can be improved to ~3.5% by correcting a layer thickness error in fabrication, and to >10% by switching to a high coupling piezoelectric such as ScAlN or LN. We expect to improve Q by further study of inner electrode material

and deposition conditions. We believe that the combination of practical layer thicknesses, flexible fabrication process, and high performance make the solidly mounted OBAR a promising approach to enabling mmWave acoustic filters.

REFERENCES

- R. Ruby, "Review and comparison of bulk acoustic wave FBAR, SMR technology," *Proc IEEE Ultrason Symp*, pp. 1029–1040, 2007, doi: 10.1109/ULTSYM.2007.262.
- [2] A. Hagelauer et al., "From Microwave Acoustic Filters to Millimeter-Wave Operation and New Applications," IEEE Journal of Microwaves, vol. 3, no. 1, pp. 484–508, Dec. 2022, doi: 10.1109/JMW.2022.3226415.
- [3] M. Hara et al., "Super-high-frequency band filters configured with air-gap-type thin-film bulk acoustic resonators," Jpn J Appl Phys, vol. 49, no. 7 PART 2, Jul. 2010, doi: 10.1143/JJAP.49.07HD13.
- [4] M. Park, J. Wang, R. Dargis, A. Clark and A. Ansari, "Super High-Frequency Scandium Aluminum Nitride Crystalline Film Bulk Acoustic Resonators," 2019 IEEE International Ultrasonics Symposium (IUS), Glasgow, UK, 2019, pp. 1689-1692, doi: 10.1109/ULTSYM.2019.8925598.
- [5] M. Kadota, F. Yamashita, and S. Tanaka, "9.5 GHz Solidly Mounted Bulk Acoustic Wave Resonator using Third Overtone of Thickness Extension Mode in LiNbO3," *IEEE International Ultrasonics Symposium*, *IUS*, vol. 2022-October, 2022, doi: 10.1109/IUS54386.2022.9957403.
- [6] J. Kramer et al., "57 GHz Acoustic Resonator with k2of 7.3 % and Q of 56 in Thin-Film Lithium Niobate," Technical Digest International Electron Devices Meeting, IEDM, vol. 2022-December, pp. 1641–1644, 2022, doi: 10.1109/IEDM45625.2022.10019391.
- [7] Izhar et al., "A K-Band Bulk Acoustic Wave Resonator Using Periodically Poled Al_{0.72}Sc_{0.28}N," *IEEE Electron Device Letters*, Jul. 2023, doi: 10.1109/LED.2023.3282170.
- [8] R. Vetury et al., "A Manufacturable AlScN Periodically Polarized Piezoelectric Film Bulk Acoustic Wave Resonator (AlScN P3F BAW) Operating in Overtone Mode at X and Ku Band," 2023 IEEE/MTT-S International Microwave Symposium - IMS 2023, pp. 891–894, Jun. 2023, doi: 10.1109/IMS37964.2023.10188141.
- [9] G. Giribaldi, P. Simeoni, L. Colombo, and M. Rinaldi, "High-Crystallinity 30% Scaln Enabling High Figure of Merit X-Band Microacoustic Resonators for Mid-Band 6G," Proceedings of the IEEE International Conference on Micro Electro Mechanical Systems (MEMS), vol. 2023-January, pp. 169–172, 2023, doi: 10.1109/MEMS49605.2023.10052384.
- [10] Y. Yang, R. Lu, T. Manzaneque, and S. Gong, "Toward Ka Band Acoustics: Lithium Niobate Asymmetrical Mode Piezoelectric MEMS Resonators," in *IFCS 2018 - IEEE International Frequency Control Symposium*, 2018. doi: 10.1109/FCS.2018.8597475.
- [11] E. T. T. Yen et al., "Integrated High-frequency Reference Clock Systems Utilizing Mirror-encapsulated BAW Resonators," IEEE International Ultrasonics Symposium, IUS, vol. 2019-October, pp. 2174–2177, Oct. 2019, doi: 10.1109/ULTSYM.2019.8925905.
- [12] Z. Schaffer, A. Hassanien, and G. Piazza, "Examination of Phonon Dissipation in 33 GHz Overmoded Bulk Acoustic Resonators," *IEEE International Ultrasonics Symposium, IUS*, vol. 2022-October, 2022, doi: 10.1109/IUS54386.2022.9958570.
- [13] Z. Schaffer, A. Hassanien, M. Masud, and G. Piazza, "Measurement of Intrinsic Mechanical Loss in Aluminum Films from 3 to 25 GHz by HBAR Spectroscopy," *IEEE International Ultrasonics* Symposium, IUS, vol. 2023-September, 2023
- [14] D. A. Feld, R. Parker, R. Ruby, P. Bradley, and S. Dong, "After 60 years: A new formula for computing quality factor is warranted," Proc IEEE Ultrason Symp, pp. 431–436, 2008, doi: 10.1109/ULTSYM.2008.0105.
- [15] C. Grünsteidl *et al.*, "Measurement of the attenuation of elastic waves at GHz frequencies using resonant thickness modes," *Appl Phys Lett*, vol. 117, no. 16, p. 164102, Oct. 2020, doi: 10.1063/5.0026367/1078501.